COMMUNICATION

Magnetic Resonance in Medicine 56:1–6 (2006)

# Chromium(VI) as a Novel MRI Contrast Agent for Cerebral White Matter: Preliminary Results in Mouse Brain In Vivo

Takashi Watanabe,* Roland Tammer, Susann Boretius, Jens Frahm, and Thomas Michaelis

**This work demonstrates that intraventricular microinjections of a low dose of potassium dichromate (0.4 μL of 10 mM solution) yield a specific contrast enhancement of white matter (WM) tracts in $T_1$-weighted 3D MRI of mouse brain in vivo. Pronounced and persistent signal increases (40–100% at 24 hr after injection) were observed in the corpus callosum, anterior commissure, fornix, and stria medullaris, as well as in the mammillothalamic tract and fasciculus retroflexus. These results suggest that the extracellular diffusion of diamagnetic chromium(VI) (Cr(VI)) after injection is followed by a tissue-specific reduction to paramagnetic Cr(V) and (III), which relies predominantly on the oxidation of myelin lipids. Because Cr(VI)-induced contrast leads to only a mild unspecific enhancement (10–20%) of gray matter (GM) structures, such as the hippocampal formation, the method reveals novel information that differs from that obtainable using other paramagnetic ions, such as manganese. Magn Reson Med 56:1–6, 2006. © 2006 Wiley-Liss, Inc.**

**Key words: myelinated nerve fibers; mouse brain; MRI; lipid oxidation; potassium dichromate**

In neuroanatomy, specific chemical reactions of lipids exposed to aqueous solutions of potassium dichromate ($K_2Cr_2O_7$ with chromium in redox state Cr(VI)) have been used for histological staining of myelin. For example, in a previous study based on Weigert-Smith-Dietrich procedures, myelin sheaths in white matter (WM) tracts in rat brain were identified by controlled chromation of lipids, which was accompanied by a simultaneous reduction of Cr(VI) (1). The present work attempts to exploit such principles for cerebral MRI of WM. The idea is based on the assumption that a reduction of diamagnetic Cr(VI) to paramagnetic Cr(V) and Cr(III) by lipid oxidation causes a shortening of the $T_1$ relaxation time of surrounding water and/or lipid protons.

Using sodium dichromate to study the metabolism of chromium species in biochemical reactions occurring on the skin of living rats, Liu and coworkers (2) demonstrated the potential of Cr(VI) for in vivo EPR spectroscopy. Similarly, the formation of Cr(V) and Cr(III) was detected by MRI after injection of sodium dichromate in the kidney and liver of a mouse in vivo (3), and of potassium chromate in the lung of a rat postmortem (4). The purposes of this first Cr(VI)-enhanced MRI study of mouse brain in vivo were to 1) examine whether a direct injection of a small amount of Cr(VI) induces a contrast enhancement detectable by $T_1$-weighted 3D MRI, 2) determine the structures highlighted in the intact living brain, and 3) discuss putative histochemical and physiological mechanisms and how they differ from other paramagnetic MRI contrast agents.

## MATERIALS AND METHODS

### Animals and Chromium Administration

Ten female mice (NMRI, 8–11 weeks old, 28–34 g) were studied in accordance with German animal protection laws after approval was granted by the responsible governmental authority. For intraventricular injection the animals were anesthetized by intraperitoneal injection of ketamine (200 mg/kg body weight) and xylazine (16 mg/kg body weight), and fixed to a stereotaxic instrument (TSE, Bad Homburg, Germany). The bregma, sagittal suture, and surface of the skull were used as references for the anterior–posterior, lateral, and ventral coordinates, respectively. A 33-gauge needle attached to a 2.5-μL Hamilton microsyringe was placed into the anterior horn of the right lateral ventricle in accordance with MR images obtained beforehand. In animals 1–5 a solution (0.4 μL, pH 5) of 10 mM potassium dichromate ($K_2Cr_2O_7$; Sigma, Taufkirchen, Germany) dissolved in physiological saline was slowly injected into the ventricle over an 8-min period. Animal 6 received a high dose of potassium dichromate (5.0 μL, 100 mM). In these experiments $Cr_2O_7^{2-}$ ions carry two negative charges with chromium in redox state Cr(VI), which is diamagnetic. To assess the putative influences of charge and redox state on the distribution of chromium ions in brain tissue, we administered animals 7 and 8 a low dose (0.4 μL, 20 mM) and a 10-fold higher dose (0.4 μL, 200 mM) of chromium chloride hexahydrate ($CrCl_3 \cdot 6\ H_2O$; Sigma, Taufkirchen, Germany), respectively. In this case $Cr^{3+}$ ions carry three positive charges and are in redox state Cr(III), which is paramagnetic. Finally, animals 9 and 10 were intraventricularly injected with Gd-DTPA (5.0 μL, 100 mM; Magnevist®, Schering, Berlin, Germany). Immediately after administration the

Biomedizinische NMR Forschungs GmbH, Max Planck Institut für Biophysikalische Chemie, Göttingen, Germany.

*Correspondence to: T. Watanabe, MD, Biomedizinische NMR Forschungs GmbH, 37070 Göttingen, Germany. E-mail: twatana@gwdg.de

Received 18 November 2005; revised 3 February 2006; accepted 22 March 2006.

DOI 10.1002/mrm.20930

Published online 9 June 2006 in Wiley InterScience (www.interscience.wiley.com).

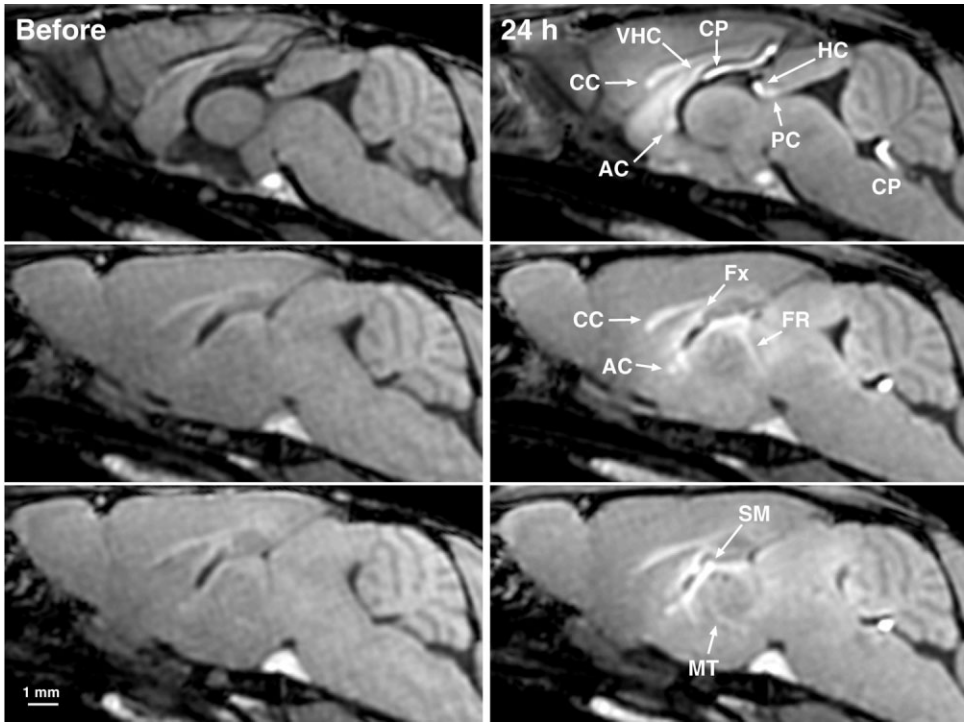


FIG. 1. (top) Midsagittal section and left-hemispheric parasagittal sections (middle) 0.3 mm and (bottom) 0.6 mm from the midline of mouse 1 (left) before as well as (right) 24 hr after Cr(VI) administration ($T_1$-weighted 3D FLASH, TR/TE = 17/7.6 ms, flip angle = 25°, isotropic resolution = 150 μm). Marked signal increases are observed in the choroid plexus (CP) as well as in WM tracts such as the corpus callosum (CC), anterior commissure (AC), ventral hippocampal commissure (VHC), habenular commissure (HC), posterior commissure (PC), fornix (Fx), and stria medullaris (SM). In addition, the fasciculus retroflexus (FR) and mammillothalamic tract (MT) are delineated.

skin incisions of the scalp were closed and covered with lidocaine hydrochloride (2% Xylocaine® gel). The animals were recovered from anesthesia and returned to their cages with unlimited access to food and water.

### MRI

MRI of the five animals with a low dose of potassium dichromate was performed before and 24 hr after Cr(VI) administration. Three animals were also scanned at 3 and 48 hr, and two animals were scanned at 72 hr. Animal 6 did not survive for 24 hr and was studied only at 3 hr after injection. The four animals that received $CrCl_3$ or Gd-DTPA were studied at 3 and 24 hr.

For MRI the animals were anesthetized and placed in the magnet as previously described (5). All measurements were carried out at 2.35 T using a MRBR 4.7/400 mm magnet (Magnex Scientific, Abingdon, UK) and a DBX system (Bruker Biospin MRI GmbH, Ettlingen, Germany) equipped with B-GA20 gradients. Radiofrequency excitation and signal reception was accomplished with use of a Helmholtz coil (i.d. 100 mm) and an elliptical surface coil (i.d. 20 × 12 mm), respectively. $T_1$-weighted 3D MRI data sets (RF-spoiled 3D fast low-angle shot (FLASH), TR/TE = 17/7.6 ms, flip angle = 25°, field of view (FOV) = 19.2 × 19.2 × 19.2 $mm^3$, matrix = 128 × 128 × 128, 16 averages, measuring time = 75 min) were acquired at 150 μm isotropic resolution (6).

For quantitative evaluations, the signal-to-noise ratio (SNR, defined as the mean MRI signal intensity of a brain region divided by the standard deviation (SD) of the noise in a part of the image outside the animal) was determined using software supplied by the manufacturer. The analysis followed a previously described strategy (5). Briefly, anatomic cross sections were obtained by multiplanar reconstructions from the original 3D MRI data sets. Standardized regions of interest (ROIs) were selected in close accordance with resolved anatomic structures. Relative SNR increases were obtained in comparison to intraindividual 3D MRI acquisitions before Cr(VI) administration.

## RESULTS

Cr(VI) is diamagnetic and has no direct effect on the relaxation rates of water protons. We confirmed this MRI silence by dissolving potassium dichromate in saline at different concentrations (data not shown). The lack of any MRI signal change reflects the fact that Cr(VI) remains unreduced if no chemical reaction partners, such as oxidizable lipids, are available.

In mice, intraventricular injections of a low dose of Cr(VI) selectively enhanced brain structures in $T_1$-weighted MRI. Figure 1 shows three sagittal sections of a 3D MRI data set of the brain of a mouse acquired before and 24 hr after administration. In the mid-sagittal section (top), major commissural fiber structures, such as the corpus callosum, anterior commissure, ventral hippocampal commissure, habenular commissure, and posterior commissure, are strongly highlighted. The parasagittal sections (middle and bottom) reveal pronounced signal increases in major WM tracts, such as the fornix and stria medullaris. In addition, and despite the fact that these WM structures are not directly exposed to cerebrospinal fluid (CSF), the mammillothalamic tract and the fasciculus retroflexus are also well delineated. Figure 2 shows corresponding transverse-to-coronal sections along these latter tracts from the same data set. Apart from the strongly enhanced corpus callosum, the images clearly identify increased signals in the mammillothalamic tract and fasciculus retroflexus on

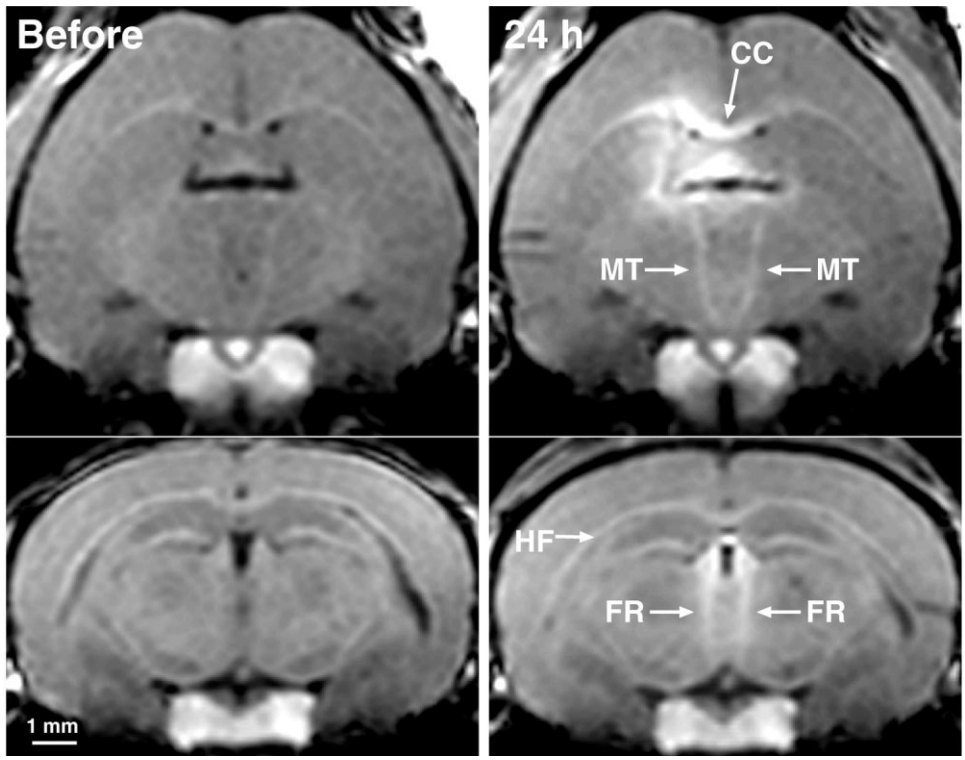


FIG. 2. Oblique sections taken from the same data set as in Fig. 1 depicting (top) the mammillothalamic tract (MT) and (bottom) the fasciculus retroflexus (FR) on both sides (left) before and (right) 24 hr after Cr(VI) administration. Note the pronounced signal increase of the corpus callosum (CC) in the ipsilateral right hemisphere, and the absence of any enhancement in the hippocampal formation (HF).

both sides. They also demonstrate the lack of specific signal increases in the hippocampal formation. Figure 3 compares Cr(VI)-induced enhancements over a period of up to 72 hr after injection. The data illustrate the early albeit still slightly diffuse labeling of WM structures, as well as their persistent and specific enhancement for at least 72 hr.

Table 1 summarizes the SNR increases in selected structures of the mouse brain 3, 24, 48, and 72 hr after Cr(VI) administration. The values represent percentage increases relative to individual precontrast 3D MRI and confirm the qualitative findings reported above. For example, at 24 hr after injection, WM tracts directly exposed to ventricular CSF yield SNR increases ranging from 50% to 100%, whereas more distant tracts still yield increases of about 40%. In contrast, gray matter (GM) structures (e.g., the thalamus and cortex) result in only a mild signal enhancement of 10–20% even when exposed to the CSF (e.g., the hippocampal formation).

Figure 4 demonstrates the results of several control experiments. In the top row the effect of diamagnetic Cr(VI) ions is compared with that of paramagnetic Cr(III) ions at an identical concentration 24 hr after injection. Whereas intraventricular injection of Cr(III) causes a mild generalized signal enhancement of about 10% ± 3% in both GM and WM, Cr(VI) leads to a much stronger and more specific structural enhancement, as shown above. Qualitatively similar results were obtained for a 10-fold higher concentration of Cr(III) ions (data not shown).

To mimic the distribution of $Cr(VI)^{2-}$ ions in brain tissue by diffusion within the interstitial fluid (ISF), the lower left image of Fig. 4 depicts the result obtained after injection of similarly charged $Gd\text{-}DTPA^{2-}$ complexes. In contrast to the commonly used intravascular injection of Gd-DTPA, which causes no signal enhancement in the brain without damage to the blood–brain barrier, the intraventricular pathway yields a pronounced signal enhancement in CSF spaces and throughout the brain. $T_1$-weighted MRI at 3 hr after administration reveals reversed $T_1$ contrast between GM and WM. This may be explained by the larger ISF volume in GM and the correspondingly higher Gd-DTPA concentration and stronger $T_1$ shortening. The effect is best seen in the cerebellum, and completely vanishes after 24 hr due to Gd-DTPA clearance (not shown). The administration of a very high dose of Cr(VI), shown in the lower right of Fig. 4, leads to a different enhancement pattern that spares CSF spaces but includes brain tissue in the vicinity of the injection site. At this early stage, GM and WM structures more distant to the ventricular system are less enhanced. The toxicity of the dosage precluded measurements at 24 hr after administration.

## DISCUSSION

The MRI results clearly indicate a tissue-specific reduction of diamagnetic Cr(VI) to paramagnetic Cr(V) and Cr(III) in structures known to consist of myelinated axonal fiber bundles. No signal increases were detected in CSF (or aqueous solutions of Cr(VI)), but increases were observed in the choroid plexus and around the unilateral injection site in the right lateral ventricle. The latter findings apply particularly to the early stages after administration and the use of very high (intolerable) concentrations of Cr(VI).

In general, the observable MRI contrast not only reflects the directional CSF flow to the third ventricle and the molecular diffusion of Cr(VI) ions in the ISF, it also predominantly depends on the specific chemical composition

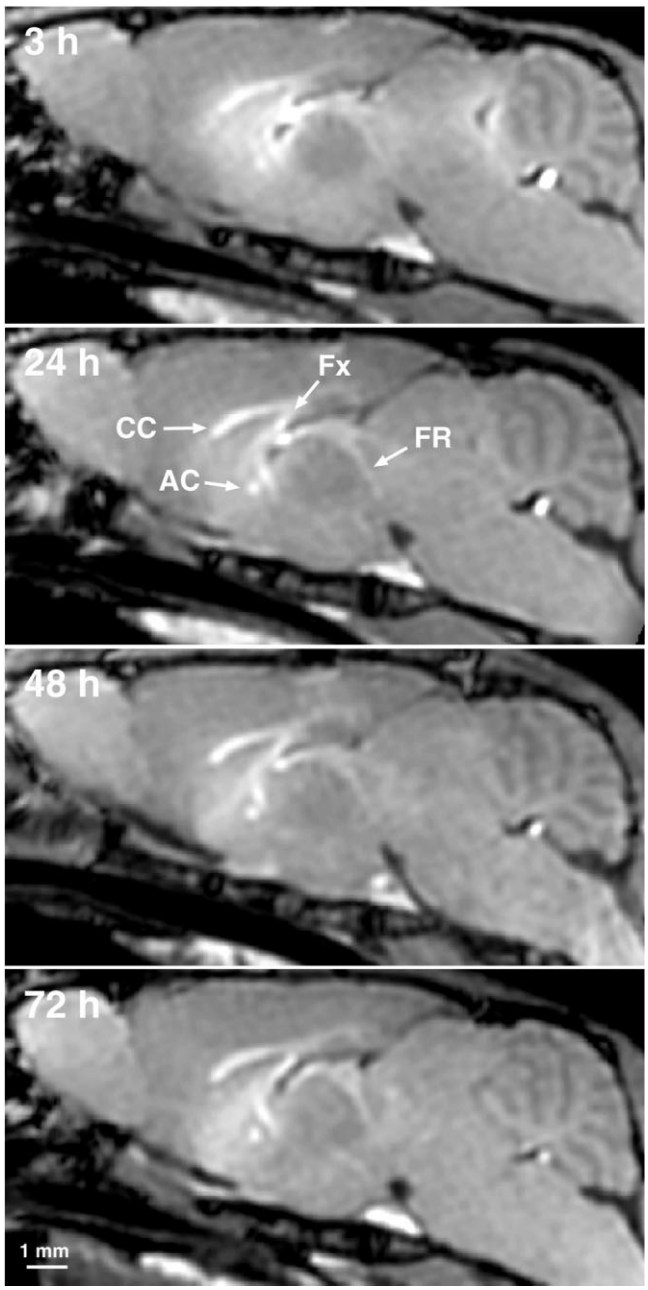


FIG. 3. Left-hemispheric parasagittal sections 0.3 mm from the midline taken from 3D MRI data sets (parameters as in Fig. 1) obtained 3, 24, and 48 hr (mouse 3), and 72 hr (mouse 5) after Cr(VI) administration. While the early studies reveal some residual diffuse enhancement in brain tissue close to the injected ventricle, the later stages highlight major WM tracts, such as the CC, AC, Fx, and FR, until at least 72 hr after administration.

of the tissue (i.e., the availability of oxidizable lipids and their reactivity toward a reduction of Cr(VI)). As far as the first mechanism is concerned, the generalized enhancement obtained after intraventricular injection and diffusion of Gd-DTPA$^{2-}$ complexes (Fig. 4, lower left) strongly suggests that the much smaller Cr(VI)$^{2-}$ ions should also have reached the entire brain parenchyma after only 3 hr. Second, the observation of only a mild unspecific signal enhancement after administration of paramagnetic Cr(III)$^{3+}$ ions (Fig. 4 upper right) further demonstrates that in the case of diamagnetic Cr(VI) the initial diffusion is dominated by the chemical process required to generate contrast. If Cr(VI) ions are in excess relative to available lipids, then the concentration of the resulting paramagnetic reaction products may be sufficient to even enhance the MRI signal of GM in regions proximal to the injection (Fig. 4, lower right). At a much lower and tolerable dose of Cr(VI), persistent enhancements were primarily observed in WM directly exposed to CSF, while smaller but still strong signal increases allowed for a delineation of more distant fibers (Figs. 1–3; Fig. 4, upper left). These findings may be explained by the specific composition of WM. The densely packed and myelinated fiber bundles contain unsaturated phospholipids that have been reported to possess a strong affinity to Cr(VI) ions (1,7). In addition, myelin has a substantially higher lipid content (>70% in dry weight) than GM (about 30% in dry weight) (8). Finally, as evidenced by the 3–72-hr time course of signal enhancements in GM and WM (Fig. 3 and Table 1), the paramagnetic reaction products are assumed to stay in the multilamellar structure of myelinated axons. In fact, while Cr(V) still has a high redox potential, Cr(III) ions are stable and most likely remain bound or complexed to oxidated compounds in myelinated fiber tracts. In agreement with earlier histochemical staining methods for visualizing chromium in tissue (1), this stability may open further applications of Cr(VI) as a dual marker for in vivo MRI and light microscopy.

Apart from the carcinogenic effect demonstrated by the high incidence of respiratory tract cancers in workers occupationally exposed to Cr(VI) compounds (3), acute toxicity of Cr(VI) due to the formation of reactive oxygen species poses a limitation of the present technique. In particular, the effect may reduce the levels of non-enzymatic antioxidants, while antioxidant enzyme activities increase as an adaptive brain response against the oxidative stress (9). Here the use of a very high dose in one animal led to clonic convulsions within 24 hr. In contrast, the injection of only 0.4 μg of Cr(VI), which is much smaller than the 1040 μg used in MRI studies of mouse liver and kidney (3), and 100 μg in rat lung (4), yielded a sufficient contrast enhancement in the brain within 24 hr after administration, with no observable behavioral alterations.

It should be noted that the need for a specific chemical reaction that converts Cr(VI) into a paramagnetic MRI contrast agent leads to marked differences in comparison with other paramagnetic ions used for contrast-enhanced MRI. For example, MRI observations in mouse brain after intracerebral injection (5) or subcutaneous application of $MnCl_2$ (10) resulted in a pattern of enhanced structures that was distinctly different from that seen here after Cr(VI) administration. Manganese is taken up by neurons through calcium channels and is subsequently transported along connected axons. Manganese-enhanced MRI after intracerebral $MnCl_2$ injections therefore strongly increases the signal intensity of the densely packed cell body assemblies in the hippocampal formation, as well as direct hippocampal projections (11). Conversely, Cr(VI)-enhanced MRI has no specific effect on GM structures, including the hippocampus, but unilateral administration strongly en-

Table 1
SNR Increases in Mouse Brain In Vivo After Injection of a Low Dose of Chromium(VI) into the Right Lateral Ventricle*

| Structure | 3 hours (n = 3) | 24 hours (n = 4) | 48 hours (n = 3) | 72 hours (n = 2) |
|---|---|---|---|---|
| WM exposed to CSF | | | | |
| Corpus callosum | 68 ± 53 | 80 ± 29 | 51 ± 29 | 50 ± 25 |
| Anterior commissure | 72 ± 27 | 80 ± 21 | 57 ± 18 | 51 ± 13 |
| Habenular commissure | 115 ± 30 | 98 ± 13 | 75 ± 15 | 77 ± 12 |
| Stria medullaris R | 85 ± 17 | 74 ± 16 | 57 ± 11 | 46 ± 12 |
| Stria medullaris L | 60 ± 17 | 57 ± 9 | 38 ± 6 | 37 ± 13 |
| Fornix R | 106 ± 42 | 91 ± 26 | 71 ± 17 | 54 ± 16 |
| Fornix L | 52 ± 13 | 54 ± 11 | 36 ± 14 | 38 ± 14 |
| WM not exposed to CSF | | | | |
| Mammillothalamic tract R | 33 ± 11 | 41 ± 8 | 31 ± 3 | 27 ± 13 |
| Mammillothalamic tract L | 30 ± 9 | 37 ± 7 | 28 ± 2 | 26 ± 10 |
| Fasciculus retroflexus R | 41 ± 14 | 40 ± 5 | 30 ± 2 | 27 ± 11 |
| Fasciculus retroflexus L | 38 ± 10 | 41 ± 4 | 31 ± 3 | 26 ± 8 |
| GM exposed to CSF | | | | |
| Hippocampal formation R | 22 ± 9 | 21 ± 10 | 3 ± 9 | 8 ± 10 |
| Hippocampal formation L | 20 ± 1 | 20 ± 11 | 7 ± 9 | 6 ± 9 |
| GM not exposed to CSF | | | | |
| Thalamus R | 19 ± 8 | 17 ± 9 | 16 ± 3 | 12 ± 9 |
| Thalamus L | 15 ± 4 | 16 ± 7 | 13 ± 4 | 10 ± 8 |
| Cerebral cortex R | 20 ± 7 | 13 ± 9 | 10 ± 4 | 5 ± 11 |
| Cerebral cortex L | 19 ± 2 | 12 ± 7 | 12 ± 4 | 5 ± 3 |

*SNR increases are given in percent relative to intraindividual precontrast MRI and represent mean values ± SD averaged across animals. WM = white matter, GM = gray matter, R = right, L = left.

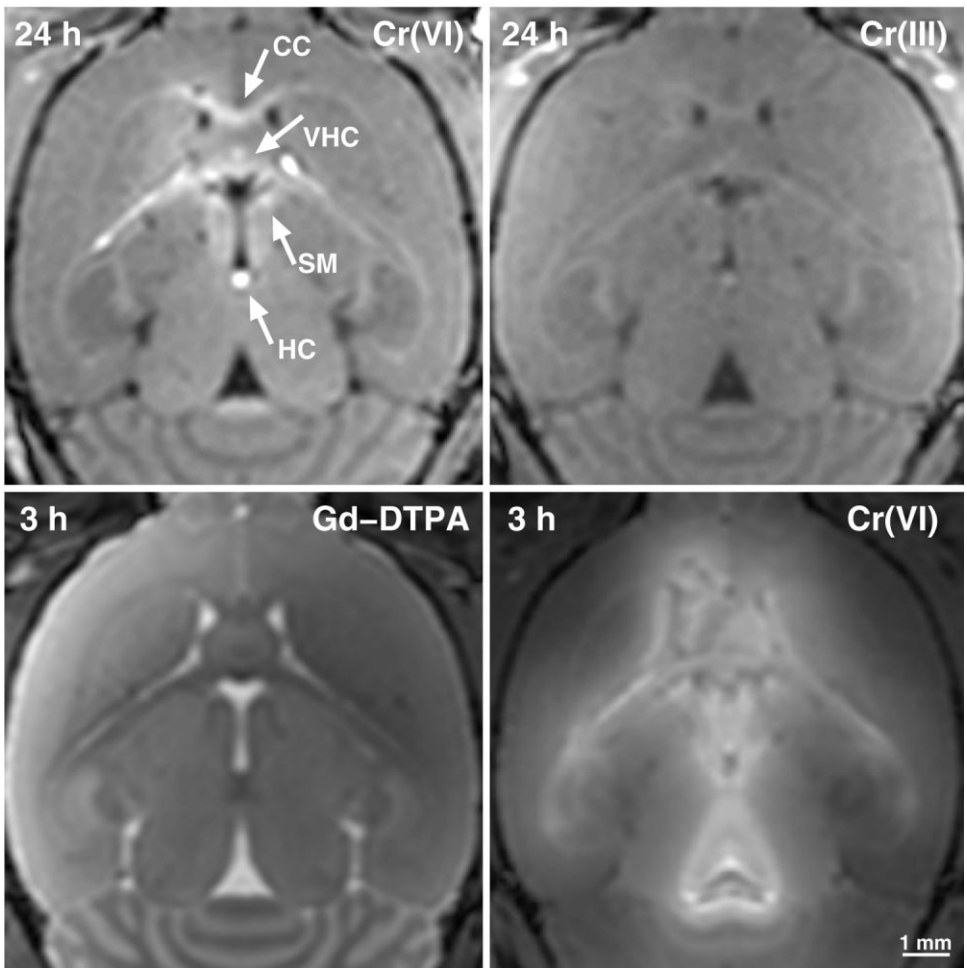


FIG. 4. Transverse sections taken from 3D MRI data sets (parameters as in Fig. 1) obtained (top) 24 hr after administration of a low dose of (left) diamagnetic Cr(VI) (mouse 4) and (right) paramagnetic Cr(III) (mouse 7) as well as (bottom) 3 hr after administration of (left) Gd-DTPA (mouse 9) and (right) a very high dose of Cr(VI) (mouse 6). While intraventricular injections of both Gd-DTPA$^{2-}$ and Cr(III)$^{3+}$ ions yield a generalized signal enhancement throughout the brain, the contrast after Cr(VI)$^{2-}$ predominantly reflects the reduction to paramagnetic Cr(V) and Cr(III) by oxidation of available lipids.

hances the corpus callosum, which is not affected by intraventricular injections of manganese. Thus, one may consider manganese as an intracellular neuronal contrast agent for functionally active brain systems, while Cr(VI) serves as an extracellular "surface" agent that labels the myelin lipids of all accessible WM structures. In view of the fact that no histochemical method is available to demonstrate manganese in tissues (12), functional mapping of neural pathways by manganese-enhanced MRI (11,13) may now be complemented by outlining WM tracts with use of Cr(VI)-induced MRI contrast.

## CONCLUSIONS

In summary, the present results show that Cr(VI) can be used to specifically enhance the $T_1$-weighted MRI signal intensity of myelinated WM tracts. These findings are in line with histological staining techniques and the high lipid content of myelin. The suggested mechanism assumes the molecular diffusion of Cr(VI) ions in the CSF and ISF to be followed by the oxidation of myelin lipids, a reduction to paramagnetic forms, and a subsequent retention of the reaction products in the multilamellar structure. It may be concluded that Cr(VI)-enhanced MRI provides new insights into the histochemistry of reactive tissue compounds that differ from the information gathered by other paramagnetic ions, such as manganese. Applications to neurodevelopment and animal models involving biochemical and structural alterations of myelin in the central nervous system are currently being investigated.

## REFERENCES

1. Pearse AGE. Histochemistry, theoretical and applied. Vol. 2, 4th ed. New York: Churchill Livingstone; 1985. p 808–811.
2. Liu KJ, Mader K, Shi X, Swartz HM. Reduction of carcinogenic chromium(VI) on the skin of living rats. Magn Reson Med 1997;38:524–526.
3. Liu KJ, Shi X. In vivo reduction of chromium(VI) and its related free radical generation. Mol Cell Biochem 2001;222:41–47.
4. Shayer R, Kinchesh P, Raffray M, Kortenkamp A. Biomonitoring of chromium(VI) deposited in pulmonary tissues: pilot studies of a magnetic resonance imaging technique in a post-mortem rodent model. Biomarkers 2004;9:32–46.
5. Watanabe T, Radulovic J, Spiess J, Natt O, Boretius S, Frahm J, Michaelis T. In vivo 3D MRI staining of the mouse hippocampal system using intracerebral injection of $MnCl_2$. Neuroimage 2004;22:860–867.
6. Natt O, Watanabe T, Boretius S, Radulovic J, Frahm J, Michaelis T. High-resolution 3D MRI of mouse brain reveals small cerebral structures in vivo. J Neurosci Methods 2002;120:203–209.
7. Morell P, Quarles RH, Norton WT. Myelin formation, structure, and biochemistry. In: Siegel GJ, Agranoff BW, Albers RW, Molinoff PB, editors. Basic neurochemistry. 5th ed. New York: Raven Press; 1994. 127 p.
8. Holczinger L. The reaction of unsaturated fats with the acid hematein test. Histochemie 1964;4:120–122.
9. Travacio M, Polo JM, Llesuy S. Chromium(VI) induces oxidative stress in the mouse brain. Toxicology 2001;162:139–148.
10. Watanabe T, Natt O, Boretius S, Frahm J, Michaelis T. In vivo 3D MRI staining of mouse brain after subcutaneous application of $MnCl_2$. Magn Reson Med 2002;48:852–859.
11. Watanabe T, Frahm J, Michaelis T. Functional mapping of neural pathways in rodent brain in vivo using manganese-enhanced three-dimensional magnetic resonance imaging. NMR Biomed 2004;17:554–568.
12. Tiffany-Castiglioni E, Qian Y. Astroglia as metal deposits: molecular mechanisms for metal accumulation, storage and release. Neurotoxicology 2001;22:577–592.
13. Koretsky AP, Silva AC. Manganese-enhanced magnetic resonance imaging (MEMRI). NMR Biomed 2004;17:527–531.